Inclusive study of strange-particle production in pp interactions at 405 GeV/c

H. Kichimi, M. Fukawa, S. Kabe, F. Ochiai, R. Sugahara, A. Suzuki, Y. Yoshimura, and K. Takahashi
KEK, National Laboratory for High Energy Physics, Oho-machi, Tsukuba-gun, Ibaraki-ken, 300-32, Japan

T. Okusawa, K. Tanahashi, M. Teranaka, and O. Kusumoto
Osaka City University, Osaka, 558, Japan

T. Konishi
Kinki University, Higashi Osaka, 577, Japan

H. Okabe and J. Yokota
Science Education Institute of Osaka Prefecture, Osaka, 558, Japan
(Received 2 January 1979)

We have studied inclusive K^0_S, Λ, and $\bar{\Lambda}$ production and strange-resonance production in the reactions $pp \to (K^0_S, \Lambda, \text{or } \bar{\Lambda}) + \pi^{\pm} + \text{anything}$ at 405 GeV/c. The observed cross sections are 7.43 ± 0.45 mb for K^0_S, 4.01 ± 0.35 mb for Λ, and 0.63 ± 0.12 mb for $\bar{\Lambda}$. From the analyses of the effective-mass distributions for the $(K^0_S\pi^{\pm})$, $(\Lambda\pi^{\pm})$, and $(\bar{\Lambda}\pi^{\pm})$ systems, the resonance production cross sections are determined as 4.1 ± 1.0 mb for $K^{*+}(890)$, 3.6 ± 1.0 mb for $K^{*-}(890)$, 3.4 ± 1.7 mb for $K^{*\pm}(1420)$, 0.67 ± 0.12 mb for $\Sigma^+(1385)$, 0.45 ± 0.09 mb for $\Sigma^-(1385)$, and 0.25 ± 0.08 mb for $\bar{\Sigma}^{\pm}(1385)$. The inclusive total and differential cross sections are discussed in comparison with data at lower energies. The direct production cross sections for pseudoscalar, vector, and tensor K mesons are estimated to be 2.3 ± 1.2, 3.4 ± 1.0, and 1.7 ± 0.8 mb, respectively. Direct pseudoscalar-K-meson production accounts for less than one-third of the total inclusive kaon production. Evidence of vector-meson dominance in inclusive meson production at high energy is indicated.

I. INTRODUCTION

Recently, a large quantity of data on inclusive particle and resonance production has been available over a wide range of momentum from medium energies to the CERN ISR energy (center-of-mass energy of 53 GeV).[1-9] These data indicate that in multihadron production process, resonance production such as $[\rho^0, f, K^*(890)]$ meson or (N^*, Y^*) baryon is dominant and vector-meson production seems remarkably important among these resonances. It has also been pointed out that about two-thirds of the final pions are produced as decay products of resonances, i.e., via indirect processes.[1,2,5] Consequently, the single-particle spectra are strongly affected by resonances produced directly in the target and projectile fragmentation regions or in the central region.

Several theoretical approaches[10-15] have been developed to investigate the multihadron production dynamics. Among these approaches, the additive quark model[10] seems to be very attractive in its simplicity. This model describes experimental data suprisingly well for cross-section ratios of particles and resonances produced at low p_T, in quite different hadronic interactions.[1,2] This model, however, has no prediction for vector/tensor ratios, and has not yet been thoroughly investigated for baryon resonance production because of scarce experimental data. The multiperipheral resonance production model[11] does give some predictions on vector/tensor ratios. Other models based on the quark-parton model[12,13] have been developed, and predictions for particle production ratios in the final state have been calculated, which agree well with recent data on π^+/π^- and K^+/K^- ratios.[16]

In these connections it should be emphasized that a systematic study of resonance production is of great interest and importance in order to understand multihadron production dynamics from the point of view of a fundamental dynamics occurring in the constituent quark system. A relatively large quantity of data[1-9] is now available on ρ^0 and f meson and Δ^{++} production, but there exists only scarce information on strange-resonance production especially in the several-hundred-GeV region.[4-7] In this report we have investigated inclusive K^0_S, Λ, and $\bar{\Lambda}$ production and strange-resonance production in the reactions $pp \to (K^0_S, \Lambda, \text{or } \bar{\Lambda}) + \pi^{\pm} + \text{anything}$ at 405 GeV/c.

II. EXPERIMENTAL PROCEDURES

The data of this experiment come from a 50 000-picture exposure of the Fermilab 30-in. hydrogen bubble chamber to a 405-GeV/c proton beam. The entire film sample of 50 000 pictures

consists of 21 000 pictures of 70-mm film and 29 000 pictures of 35-mm film. Measured data of these two kinds of film were carefully checked and compared with each other by the analysis of mass distributions for accepted K^0_S and Λ events. After confirming that the two measurements have no systematic difference from each other, the two data samples were combined for further analysis.

A. Scanning and measuring

Two independent scans were performed over the entire film sample to search for events with one or more vees associated with the primary vertex. Vee events with a clear signature of an electron or positron spiral were excluded. A third scan was made by physicists to resolve all conflicts between the two initial scans, and the combined efficiency for both scans was found to be more than 98%. Measurements of vee tracks and secondary tracks were carried out on conventional manual projectors. Secondary tracks were track-matched by physicists before measuring, and as many tracks as possible were measured, even those with an opening angle of less than one degree with respect to the incident beam direction. In the analysis of 35-mm film, premeasurements of beam tracks and vee tracks were done to select events associated with genuine vees, such as K^0_S, Λ, and $\bar{\Lambda}$. Full measurements for these selected events were then performed. The measured events were processed through the reconstruction program TVGP. Track residuals were restricted to be less than 30 μm on film. A measurement was repeated up to three times for events which failed in TVGP, and 1465 events associated with 1759 vees were obtained. The measuring efficiencies of events and vees were found to be 90% and 87%, respectively.

B. Particle identification

Vee events were identified as γ, K^0_S, Λ, or $\bar{\Lambda}$ from the p_T^- distribution and the mass distribution, for each mass hypothesis (γ, K^0_S, Λ, or $\bar{\Lambda}$), using the TVGP results. In this analysis, p_T^- was defined as the transverse momentum of the negative track (the positive track for the $\bar{\Lambda}$ hypothesis) with respect to the vee momentum direction. The $p_T^{e^-}$ distribution and the mass distribution of all events for the hypotheses $\gamma \to e^+e^-$ are shown in Figs. 1(a) and 1(b). Figure 1(a) shows clear peaks at $p_T^{e^-} = 0$, 100, and 200 MeV/c, corresponding to the kinematic boundaries of γ, ($\Lambda, \bar{\Lambda}$), and K^0_S decays in their rest systems. The shaded areas show events with $p_T^{e^-}$ less than 15 MeV/c, which may be clearly identified as γ events. In Figs. 2(a), 2(b),

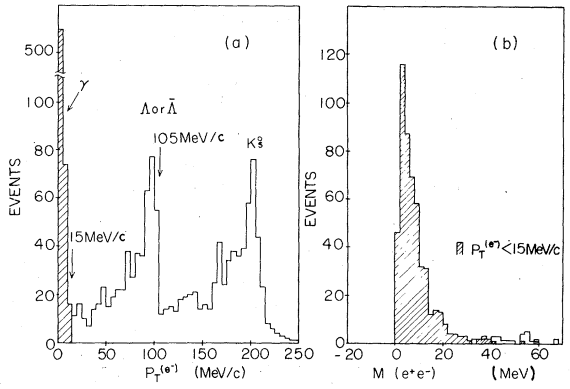

FIG. 1. (a) $p_T^{e^-}$ distribution and (b) mass distribution of all events for the hypothesis $\gamma \to e^+e^-$ conversion. The shaded area shows the events with $p_T^{e^-}$ less than 15 MeV/c, which are clearly identified as γ events.

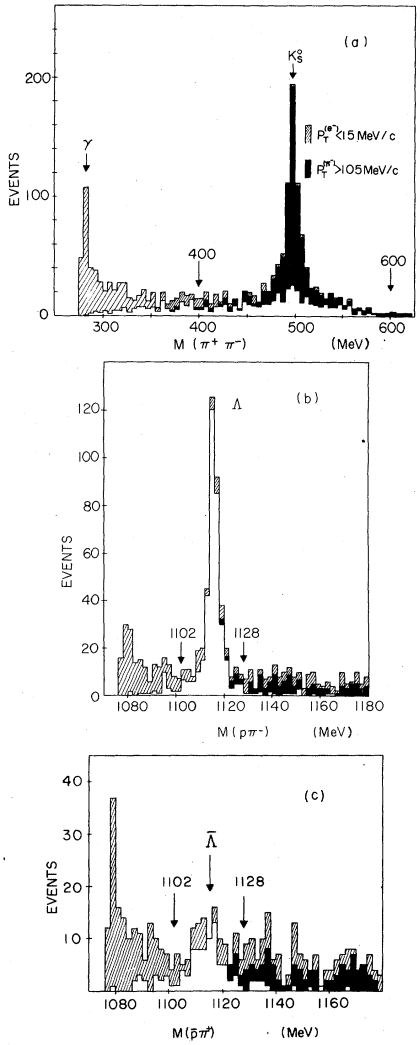

FIG. 2. Mass distributions for the hypotheses (a) $K^0_S \to \pi^+\pi^-$, (b) $\Lambda \to p\pi^-$, and (c) $\bar{\Lambda} \to \bar{p}\pi^+$. The dark area shows the events with $p_T^{\pi^-}$ greater than 105 MeV/c.

and 2(c) are shown the mass distributions for the hypotheses $K^0_S \to \pi^+\pi^-$, $\Lambda \to p\pi^-$, and $\bar{\Lambda} \to \bar{p}\pi^+$, respectively. The shaded areas indicate the γ events mentioned above. The dark areas indicate the events with $p_T^{\pi^-}$ greater than 105 MeV/c, which show a clear peak centered at the K^0_S mass and can be uniquely identified as K^0_S from Q-value consideration [Fig. 2(a)]. The events remaining unmarked in Fig. 2(a) correspond to K^0_S-Λ or K^0_S-$\bar{\Lambda}$ unseparated events. Accordingly, the first selection criteria were set for γ, K^0_S, Λ, or $\bar{\Lambda}$ as follows:

γ: $p_T^{e^-} \leq 15$ MeV/c,
K^0_S: $p_T^{\pi^-} \geq 105$ MeV/c or $400 \leq M(\pi^+\pi^-) \leq 600$ MeV,
Λ: $p_T^{\pi^-} < 105$ MeV/c and $1102 \leq M(\pi^- p) \leq 1128$ MeV,
$\bar{\Lambda}$: $p_T^{\pi^+} < 105$ MeV/c and $1102 \leq M(\pi^+ \bar{p}) \leq 1128$ MeV.

The fitted pattern of events for each hypothesis is given in Table I. There is no ambiguity between the Λ and $\bar{\Lambda}$ hypotheses, while some ambiguities for the K^0_S-Λ hypotheses and the K^0_S-$\bar{\Lambda}$ hypotheses remain. Those events, shown as the unmarked areas in Figs. 2(b) and 2(c), have clear peaks in Λ and $\bar{\Lambda}$ mass regions and indicate a small contamination from K^0_S events. The mass distributions for these K^0_S-Λ and K^0_S-$\bar{\Lambda}$ ambiguous events were further analyzed to resolve ambiguities, and the final selection criteria were set as follows:

K^0_S-Λ ambiguities; events with the mass $495 \leq M(\pi^+\pi^-) \leq 501$ MeV are assigned as K^0_S, and the remaining events as Λ.

K^0_S-$\bar{\Lambda}$ ambiguities; events with the mass $475 \leq M(\pi^+\pi^-) \leq 525$ MeV as K^0_S and the remaining events as $\bar{\Lambda}$.

γ ambiguities; all events with $p_T^{e^-} \leq 15$ MeV are assigned as γ.

The selection pattern of events and the contamination pattern are also shown in Table I. We also checked that the ionization loss on vee tracks was consistent with each mass hypothesis. In Fig. 3 the mass distributions and p_T^{π} distributions are shown for events selected as K^0_S, Λ, and $\bar{\Lambda}$. The solid lines show the curves estimated from the assumption of the isotropic decay in the vee rest system. The association angle was restricted to be less than 75 mrad, which is defined as the angle between the vee momentum and the direction of the vector going from the primary vertex to the vee vertex.

C. Fiducial volume and decay probability

Fiducial cuts on both the primary and the vee vertices were imposed in order to calculate the decay probability. The primary vertex fiducial volume was defined as $-2 \leq x \leq 16$ cm, $-24 \leq y$

TABLE I. Selection of γ, K^0_S, Λ, and $\bar{\Lambda}$.

(a) Selection of γ, K^0_S, Λ, and $\bar{\Lambda}$ events

	Unique fits	Multiple fits: γ with $K^0_S/\Lambda/\bar{\Lambda}$	Multiple fits: K^0_S-Λ	Multiple fits: K^0_S-$\bar{\Lambda}$	No. of selected events	No. of events used in analysis [a]	Average weight
Fitted events	1256	190	255	58	1759	...	...
γ	411	190			601	...	...
K^0_S	666		16	35	717	488	1.61
Λ	94		239		333	242	1.67
$\bar{\Lambda}$	11			20	31	28	2.28
No fit	74			3	77	...	...

(b) Contamination pattern

Hypothesis	No. of selected events	Contamination [b]: γ	K^0_S	Λ	$\bar{\Lambda}$	Sum	Ratio
K^0_S	717	17	...	30	5	52	7%
Λ	333	8	20	...	...	28	8%
$\bar{\Lambda}$	31	1	5	...	...	6	19%
	1081						

[a] These numbers of events were obtained after various cuts: (i) association angle less than 75 mrad, (ii) $x_F < 0.0$, and (iii) restricted fiducial volume. See text.

[b] Estimation from p_T^{π} and mass distribution analyses.

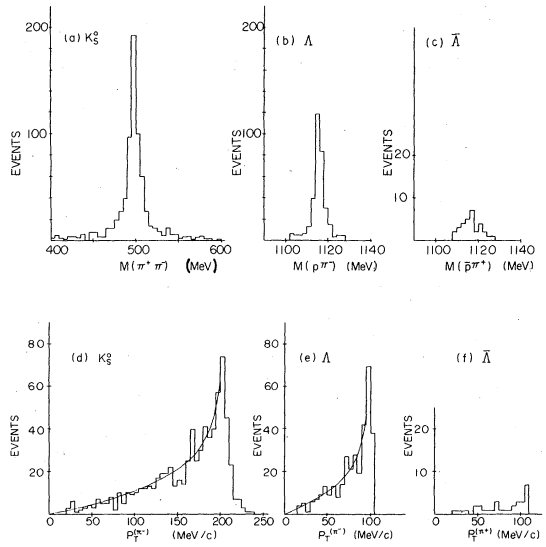

FIG. 3. Mass distributions (a)–(c) and p_T^{π} distributions (d)–(f) for events selected as K_S^0, Λ, and $\bar{\Lambda}$, respectively. The solid lines in (d) and (e) show the curves estimated from the assumption of the isotropic decay in the vee rest system.

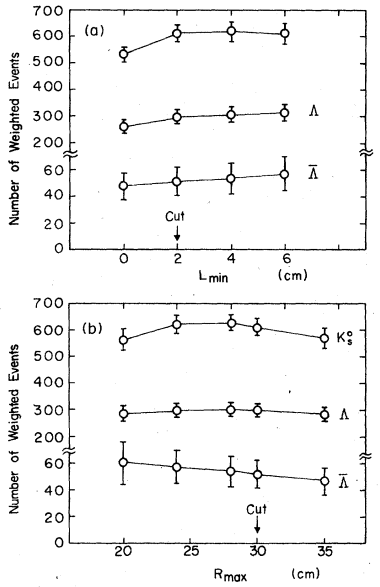

FIG. 4. The weighted number of events as a function of (a) L_{min} and (b) R_{max}.

≤ 28 cm, and $-22 \leq z \leq -14$ cm. The origin is at the center of the chamber front glass with the beam going along the negative y direction and z negative in the chamber. The vee vertex fiducial volume was defined as $-24 \leq z \leq -14$ cm and $R_{max} = (x^2+y^2)^{1/2} \leq 30$ cm. To each event in the fiducial volume the following weight was applied:

$$\text{Weight} = (e^{-L_{min}/L_0} - e^{-L_{pot}/L_0})^{-1},$$

where L_{pot} is the potential length of the vee (i.e., the path length from the primary vertex to the edge of the fiducial volume), L_{min} is the minimum length permitted between the primary and vee vertices defined as 2 cm, and L_0 is the decay length of the vee particle given as $L_0 = c\tau p_V/m_V$. Figures 4(a) and 4(b) show the weighted number of K_S^0, Λ, or $\bar{\Lambda}$ events as a function of L_{min} and R_{max}, respectivily, where the primary vertex is restricted to the region $-20 < y < 20$ cm. The cuts $L_{min} = 2$ cm and $R_{max} = 30$ cm are shown to be reasonable. The average weight for a K_S^0, Λ, or $\bar{\Lambda}$ going backward in the center-of-mass system is given in Table I. The normalized decay length (L/p) distributions for events selected as K_S^0, Λ, and $\bar{\Lambda}$ are shown in Fig. 5, where L is the decay length and p is the laboratory momentum of vee. The slope values are steeper than $c\tau/m_V$ because of the restriction of the fiducial volume. The solid curves calculated from decay simulation in the same restricted fiducial volume show good fits to the distributions for real events.

After these procedures, 702 events associated with 758 vees are obtained, which include 488 K_S^0's, 242 Λ's, and 28 $\bar{\Lambda}$'s going backward in the c.m. system in the restricted fiducial volume. The cross sections obtained after corrections for decay probabilities, decay branching ratios, and some losses in scanning and measuring are tabulated in Table II.

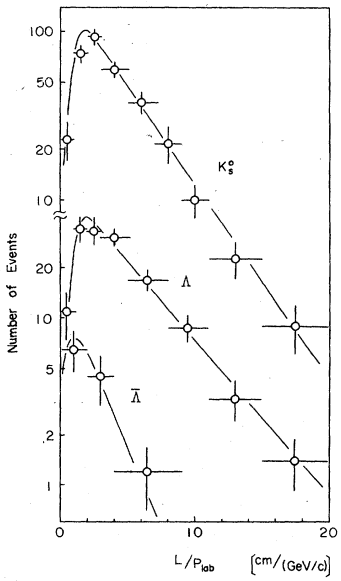

FIG. 5. Normalized decay-length distributions for selected K_S^0, Λ, and $\bar{\Lambda}$ events in a restricted fiducial volume. The solid lines are calculated from decay simulation in the same fiducial volume.

TABLE II. Topological cross sections for $p+p \rightarrow (K_S^0, \Lambda, \text{or } \bar{\Lambda})+X$.

Topology	K_S^0 events Raw no. of events	$\sigma_n(K_S^0)$ (mb)	Λ events Raw no. of events	$\sigma_n(\Lambda)$ (mb)	$\bar{\Lambda}$ events Raw no. of events	$\sigma_n(\bar{\Lambda})$ (mb)
2	8	0.12 ±0.04	6	0.09 ± 0.04	0	
4	50	0.77 ±0.11	22	0.43 ± 0.09	3	0.16 ± 0.06
6	79	1.19 ±0.13	36	0.59 ± 0.10	4	
8	84	1.31 ±0.14	49	0.75 ± 0.11	2	0.16 ± 0.06
10	98	1.44 ±0.15	46	0.84 ± 0.12	6	
12	62	0.91 ±0.12	33	0.52 ± 0.09	7	0.20 ± 0.07
14	47	0.73 ±0.11	31	0.47 ± 0.08	1	
16	30	0.50 ±0.09	13	0.20 ± 0.06	2	0.11 ± 0.05
18	11	0.16 ±0.05	3	0.06 ± 0.03	3	
20	15	0.24 ±0.06	3	0.04 ± 0.02		
22	2	0.024 ± 0.017				
24	2	0.028 ± 0.020				
Total	488	7.43 ±0.45	242	4.01 ± 0.35	28	0.63 ± 0.12

D. Secondary tracks

Within the selected 702 events, the 4940 secondary tracks passed TVGP reconstruction after a cut such that its residual was less than 30 μm. Ionization loss for low-momentum secondary tracks up to about 1.4 GeV/c was checked by physicists in order to discriminate positive pions from protons. Positive tracks with momenta greater than 1.4 GeV/c are taken to be π^+ and all negative tracks to be π^-. The polar, azimuthal angles and $x_F = p_L^{\text{c.m.}}/p_{\text{max}}^{\text{c.m.}}$ (the Feynman variable) for secondary tracks were also analyzed to check measuring biases on tracks with high momenta. These distributions show no bias for measured secondary tracks with x_F less than 0.05. We use only these tracks in further analysis.

E. Topological cross sections and beam path length

Out of 50 000 pictures, 4129 pictures were specially scanned to find the beam path length and topo-

TABLE III. Average number of K_S^0, Λ, and $\bar{\Lambda}$ per inelastic collision.

(a) Average number of K_S^0, Λ, and $\bar{\Lambda}$

Topology	$\sigma_n^{\text{inel}}(pp)$ (mb)	$\langle n_{K_S^0} \rangle$	$\langle n_\Lambda \rangle$	$\langle n_{\bar{\Lambda}} \rangle$
2	2.7 ±0.1	0.04 ±0.02	0.03 ±0.01	
4	4.46 ± 0.41	0.17 ±0.03	0.10 ±0.02	0.016 ± 0.006
6	5.49 ± 0.41	0.22 ±0.03	0.11 ±0.02	
8	6.02 ± 0.43	0.22 ±0.03	0.13 ±0.02	0.015 ± 0.006
10	4.89 ± 0.39	0.29 ±0.04	0.17 ±0.03	
12	3.34 ± 0.32	0.28 ±0.05	0.16 ±0.03	0.036 ± 0.013
14	2.33 ± 0.27	0.32 ±0.06	0.20 ±0.04	
16	1.33 ± 0.20	0.38 ±0.09	0.15 ±0.05	
18	0.80 ± 0.16	0.37 ±0.10	0.09 ±0.04	0.052 ± 0.025
20	0.29 ± 0.09			
22	0.22 ± 0.09	0.13 ±0.08		
24	0.16 ± 0.07			
Total	32.0 ±1.0	0.232 ± 0.011	0.125 ± 0.008	0.020 ± 0.004

(b) Parameters for fits to the form $\langle n_V \rangle = \alpha + \beta n_-$.

Parameter	K_S^0	Λ	$\bar{\Lambda}$
α	0.076 ± 0.016	0.048 ± 0.011	0.0067 ± 0.0088
β	0.047 ± 0.006	0.025 ± 0.004	0.0040 ± 0.0027
	$n_- \leq 9$	$n_- \leq 7$	$n_- \leq 8$
χ^2/DF	10.83/7	6.82/6	1.89/2

logical cross sections. We restricted the scanning to events with four or more than four charged tracks. Each picture was classified as good or bad according to the picture quality. The picture was defined as good if it had less than 15 clear incident beams and no complicated noise due to γ-ray conversions or overlapping multiprong events. It was found that 75% of the pictures qualified as good pictures. The fiducial length was defined as 47 cm, and the average number of incident beams per pictures was found to be 5.2, which corresponds to 2.27 μb/ev for the entire film sample. The topological cross sections obtained are shown in Table III, where the cross section for $n_{ch} = 2$ was taken from the value in Ref. 17.

III. INCLUSIVE K^0_S, Λ, AND $\bar{\Lambda}$ PRODUCTION

A. Cross sections

The cross sections for K^0_S, Λ, and $\bar{\Lambda}$ production are calculated on the basis of the observed numbers of K^0_S, Λ, and $\bar{\Lambda}$ events as discussed in Sec. II C, and are given in Table II. The associated topological cross sections are also given. The total cross sections obtained are $\sigma(K^0_S) = 7.43 \pm 0.45$ mb, $\sigma(\Lambda) = 4.01 \pm 0.35$ mb, and $\sigma(\bar{\Lambda}) = 0.63 \pm 0.12$ mb. Table III shows the average numbers of K^0_S, Λ, and $\bar{\Lambda}$ per inelastic collision. The observed average numbers are $\langle K^0_S \rangle = 0.232 \pm 0.011$, $\langle \Lambda \rangle = 0.125 \pm 0.008$, and $\langle \bar{\Lambda} \rangle = 0.020 \pm 0.004$, where $\sigma^{inel}(pp) = 32.0 \pm 1.0$ mb was used. The cross sections of K^0_S, Λ, and $\bar{\Lambda}$ are plotted in Fig. 6(a) as a function of the center-of-mass energy squared s together with data at lower energies.[3,9] The cross section of $\bar{\Lambda}$ production is relatively small, but increases rapidly with energy. In contrast, the increase of the cross section of Λ production seems to be flattening above 100 GeV/c. The average numbers of K^0_S, Λ, and $\bar{\Lambda}$ per inelastic collision are also plotted in Fig. 6(b). Linear increases of the average numbers of K^0_S, Λ, and $\bar{\Lambda}$ as a function of $\ln(s)$ are observed in the incident momentum region above 100 GeV/c. The slope values are obtained by fitting the form $\langle V \rangle = \alpha + \beta \ln(s)$ above 100 GeV/c (Ref. 9):

$$\langle K^0_S \rangle = -(0.29 \pm 0.05) + (0.079 \pm 0.009) \ln(s) \qquad (\chi^2/\mathrm{DF} = 1.95/3),$$

$$\langle \Lambda \rangle = (0.026 \pm 0.051) + (0.014 \pm 0.008) \ln(s) \qquad (\chi^2/\mathrm{DF} = 1.63/3),$$

and

$$\langle \bar{\Lambda} \rangle = -(0.044 \pm 0.018) + (0.010 \pm 0.003) \ln(s) \qquad (\chi^2/\mathrm{DF} = 1.54/2),$$

where DF stands for the number of degrees of

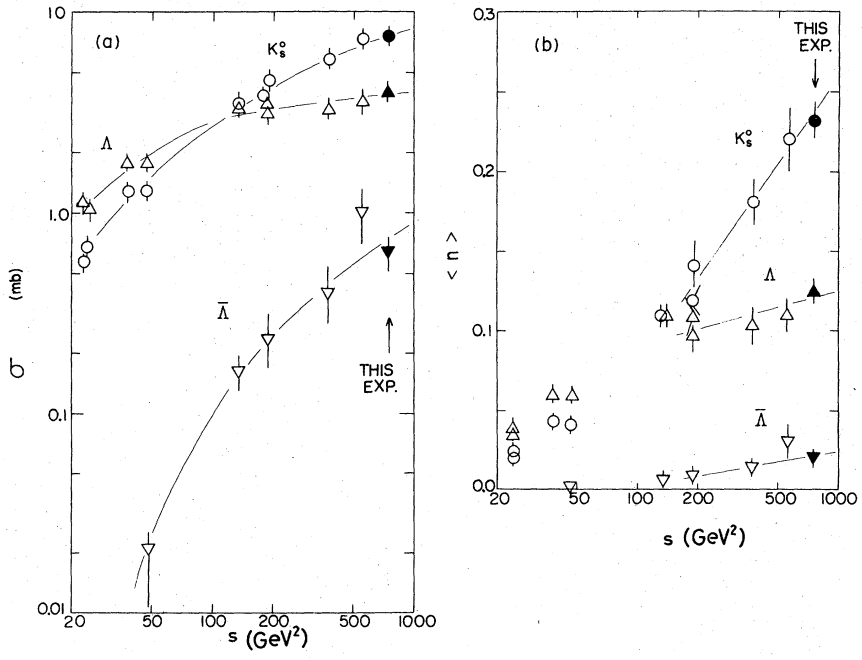

FIG. 6. (a) Cross sections for inclusive K^0_S, Λ, and $\bar{\Lambda}$ production, and (b) average numbers of K^0_S, Λ, and $\bar{\Lambda}$ per inelastic collision, both as a function of the c.m. energy squared s. The data at lower energies come from Refs. 3 and 9. The curves in (a) are drawn to guide the eye. The straight lines in (b) are linear fits to the data above 100 GeV/c (p_{inc}).

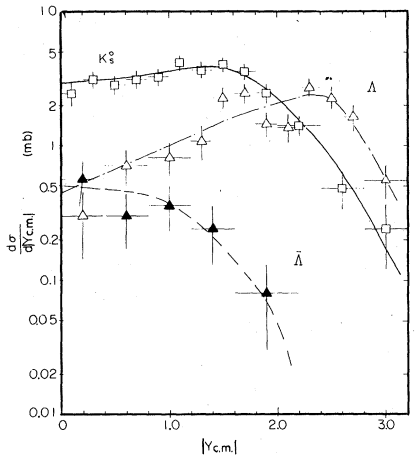

FIG. 7. Rapidity distributions for K^0_S, Λ, and $\bar{\Lambda}$ production in the c.m. system. The curves are drawn to guide the eye.

freedom. The ratios of these slope values may be used to obtain the production ratios of the corresponding particles in the central region. These ratios are obtained as

$$\beta_{K^0_S}: \beta_\Lambda: \beta_{\bar{\Lambda}} = 1: 0.18 \pm 0.10: 0.13 \pm 0.04,$$

which are in good agreement with the values 1: $\frac{1}{6}$: $\frac{1}{6}$, predicted by the additive quark model[10] for meson/baryon/antibaryon production in the central region.

We have also made an independent study of the production ratios of K^0_S, Λ, and $\bar{\Lambda}$ in the central region by using the rapidity distributions. Figure 7 shows the rapidity distributions in the center-of-mass system for K^0_S, Λ, and $\bar{\Lambda}$ production. A central plateau for K^0_S around $|y_{c.m.}| = 2.0$ is observed, which shows a slight falloff towards $y_{c.m.} = 0$. The distribution for Λ production shows a broad bump near $|y_{c.m.}| = 2.5$ and levels off slowly towards $y_{c.m.} = 0$. $\bar{\Lambda}$ production is observed to occur dominantly in the central region and shows a central plateau for $|y_{c.m.}| \leq 0.8$, where the $\Lambda/\bar{\Lambda}$ ratio is found to be 1.18 ± 0.46, consistent with unity. In the region $|y_{c.m.}| \leq 1.2$, the ratios for K^0_S, Λ, and $\bar{\Lambda}$ production are found to be 1: 0.19 ± 0.04: 0.13 ± 0.03. These results are again in good agreement with the prediction of the quark model.

The topological cross sections are plotted in Fig. 8(a). The maxima of the distributions for K^0_S and Λ associated events ($n_{ch} = 10$), and possibly for $\bar{\Lambda}$ events, seem to be larger than that of the charged multiplicity distribution ($n_{ch} = 8$). This indicates that strange-particle production occurs predominantly in the events having higher than average charged multiplicity. Table III(a) shows the average number of K^0_S's, Λ's, and $\bar{\Lambda}$'s associated with each topology. Linear correlations are observed in all cases, as shown in Figs. 8(b) and 8(c). The curves show results of a fit to the form $\langle V \rangle_{n_-} = \alpha + \beta n_-$, where $\langle V \rangle$ is the average number of K^0_S's, Λ's, and $\bar{\Lambda}$'s and n_- is the negative charged multiplicity. The results are shown in Table III (b). These slope parameters seem to be proportional to the corresponding average number of particles $\langle V \rangle$, as follows:

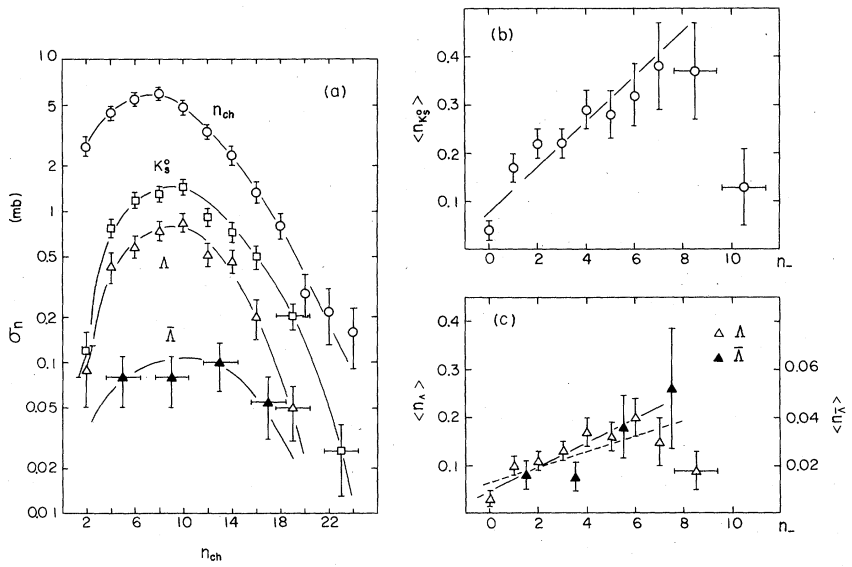

FIG. 8. (a) Topological cross sections for charged particles n_{ch}, K^0_S, Λ, and $\bar{\Lambda}$. (b) Average number of K^0_S as a function of topology. (c) The same as (b) for Λ and $\bar{\Lambda}$. The curves in (a) are drawn to guide the eye. The straight lines in (b) and (c) are linear fits to the data.

$\langle K^0_S\rangle_{n_-}/\langle K^0_S\rangle = (0.33\pm0.07) + (0.20\pm0.03)n_-$ $(n_- \leq 9)$,

$\langle\Lambda\rangle_{n_-}/\langle\Lambda\rangle = (0.38\pm0.09) + (0.20\pm0.03)n_-$ $(n_- \leq 7)$,

and

$\langle\overline{\Lambda}\rangle_{n_-}/\langle\overline{\Lambda}\rangle = (0.34\pm0.44) + (0.20\pm0.14)n_-$ $(n_- \leq 8)$.

Averaging over these three relations, one may obtain $\langle V\rangle_{n_-} = (0.35 + 0.20\,n_-)\,\langle V\rangle$. This result indicates that the topological cross sections for K^0_S, Λ, and $\overline{\Lambda}$ production have a common distribution function of $\sigma_n(V)/\langle V\rangle = (0.35 + 0.20n_-)\,\sigma_n$, where σ_n is the charged topological cross section.

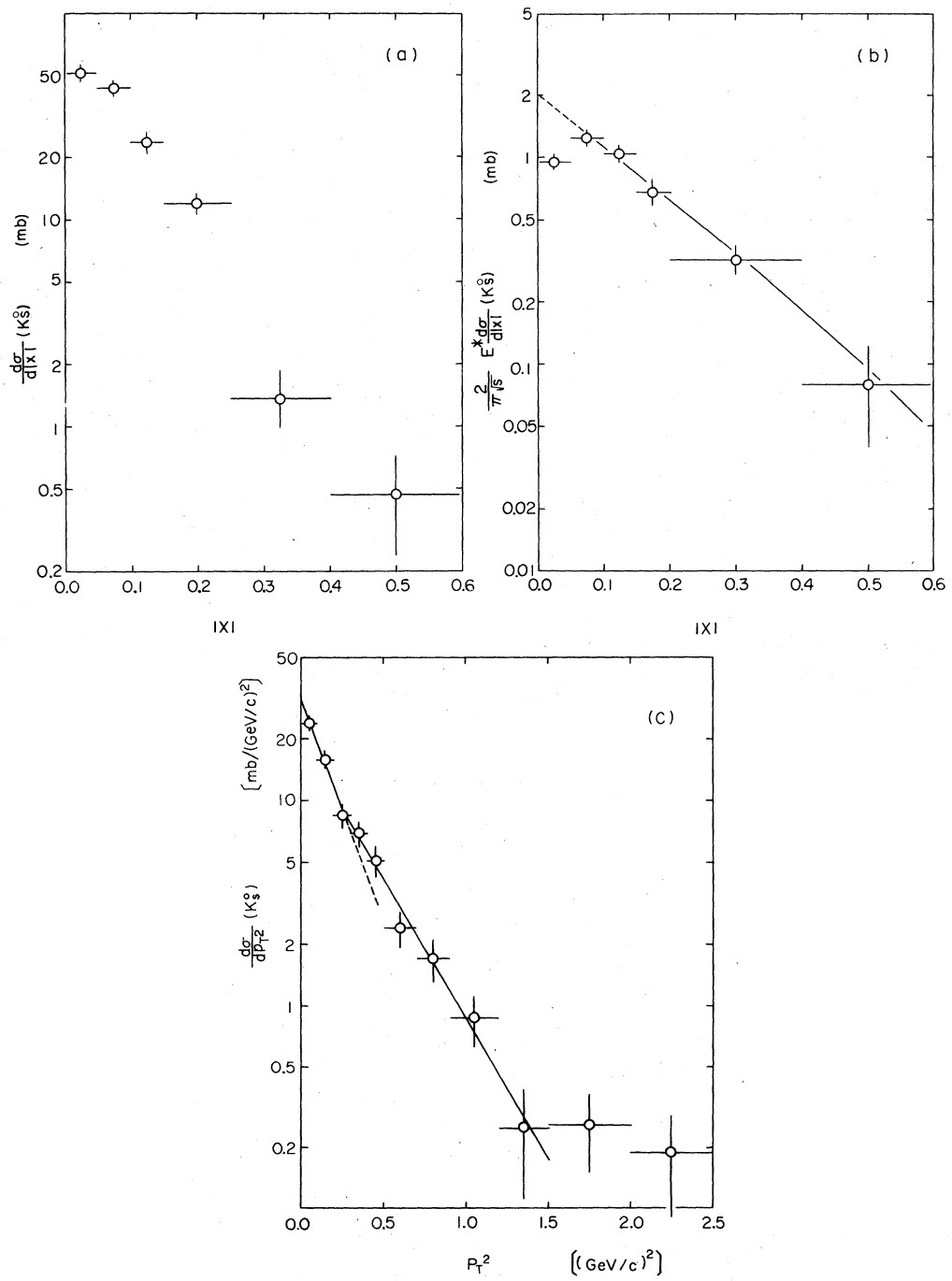

FIG. 9. Differential cross sections for inclusive K^0_S production. (a) $d\sigma/d\,|x|$ and (b) $(2/\pi\sqrt{s})\int (E^*d^2\sigma/d\,|x|\,dp_T^{\,2})dp_T^{\,2}$. The solid line is drawn from the function $E^*d\sigma/d\,|x| \propto [(1-x)^3+2(1-x)^7]$. (c) $d\sigma/dp_T^{\,2}$, where the straight lines show the result of fitting to a two-slope form.

B. Inclusive spectra for K_S^0 production

The differential cross sections of K_S^0 in terms of the scaling variable x and p_T^2 are shown in Fig. 9. Figures 9(a) and 9(b) show the noninvariant and the invariant $|x|$ distributions, respectively. The present data scale within errors when compared with other Fermilab data at lower energies.[3,9]

The $|x|$ distribution is consistent with a prediction of the constituent-interchange model

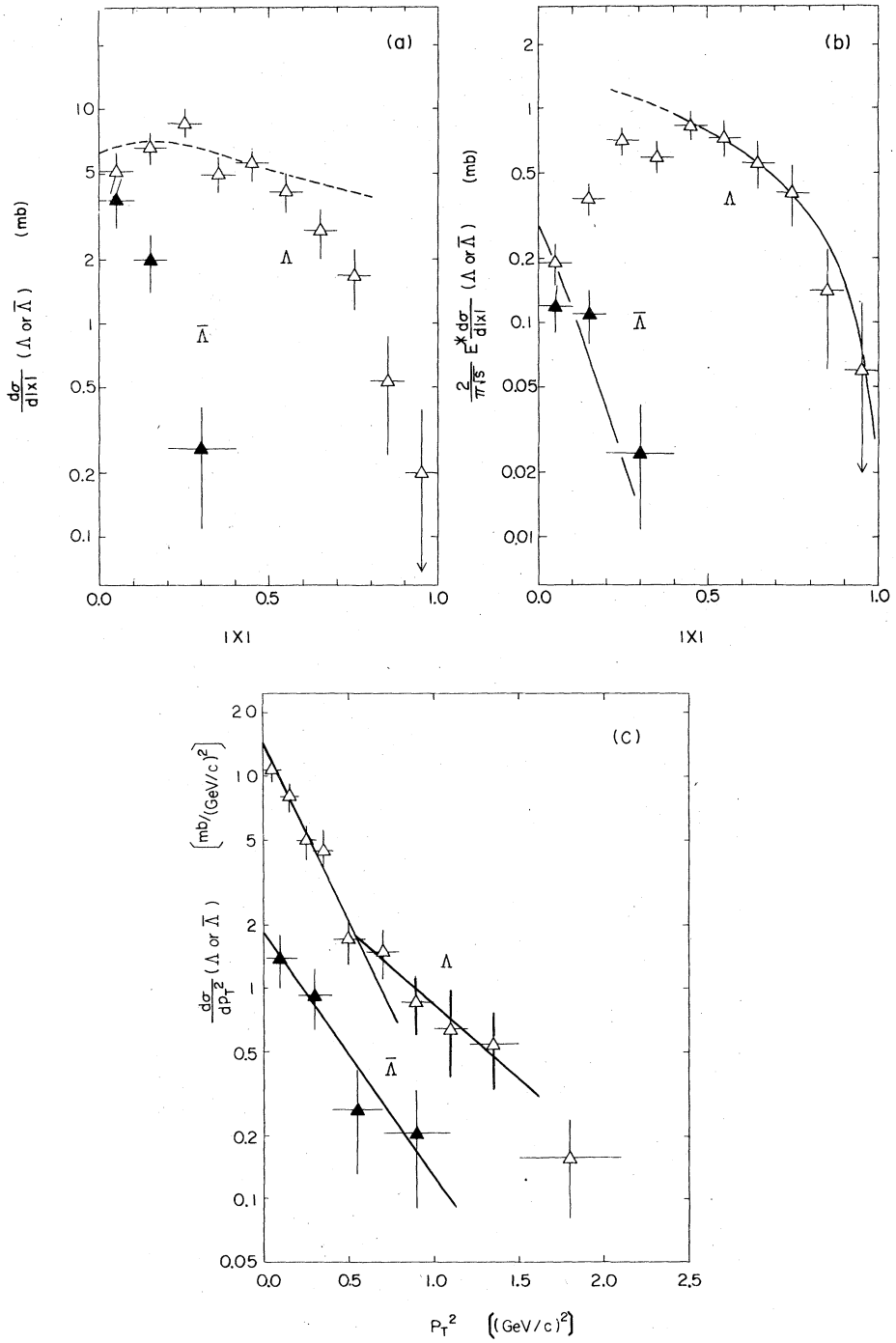

FIG. 10. Differential cross sections for inclusive Λ and $\bar{\Lambda}$ production. (a) $d\sigma/d|x|$ and (b) $(2/\pi\sqrt{s})\int (E^* d^2\sigma/d|x| \times dp_T^2) dp_T^2$. The solid lines are drawn from the functions $E^* d\sigma/d|x| \propto (1-|x|)$ for Λ and $(1-|x|)^9$ for $\bar{\Lambda}$. (c) $d\sigma/dp_T^2$, where the straight lines show the results of fitting to a two-slope form.

(CIM).[13] In the CIM inclusive spectra are described as $E^*d^3\sigma/dp^3 = R(1-x)^F$ for $p_T \simeq 0$, where F is related to the minimal number of spectator quarks by $F = 2p-3$. Recent data at Fermilab[18] have reported good agreement with the idea of dimensional counting as presented in the CIM. The solid line in Fig. 9(b) illustrates the prediction for our data:

$$E^*\frac{d\sigma(K_S^0)}{d|x|} \propto [(1-|x|)^3 + 2(1-|x|)^7],$$

assuming $\sigma(K^0) = \sigma(\bar{K}^0)$, which is a combined functional form of $(1-|x|)^3$ for K^0 and $(1-|x|)^7$ for $\bar{K}^0$, since K_S^0 is a mixed state of K^0 and $\bar{K}^0$. Our data also show qualitative agreement with the power behavior $F = 2p-3$.

Figure 9(c) shows the $p_T{}^2$ distribution. The slope value is calculated as 3.59 ± 0.18 (GeV/c)$^{-2}$ in the region $p_T{}^2 \leq 1.5$ (GeV/c)^2 with $\chi^2/\mathrm{DF} = 8.37/7$. However, a break near 0.3 (GeV/c)^2 is observed, and a fit for a two-slope form yields 4.96 ± 0.71 (GeV/c)$^{-2}$ for $p_T{}^2 \leq 0.3$ (GeV/c)^2 and 3.12 ± 0.34 (GeV/c)$^{-2}$ for $0.3 < p_T{}^2 \leq 1.5$ (GeV/c)^2 with $\chi^2/\mathrm{DF} = 2.68/5$. This steep slope in the small-$p_T{}^2$ region can be attributed to resonance decay effects,[1,8] such as $K^*(890)$ and $K^*(1420)$.

C. Inclusive spectra for Λ and $\bar{\Lambda}$ production

The differential cross sections for Λ and $\bar{\Lambda}$ production are shown in Figs. 10(a)–10(c). Λ production scales within errors, when compared with other Fermilab data at lower energies.[3,9] Λ production occurs in the wide range of $|x|$ from 0.0 to 1.0, and the invariant distribution as shown in Fig. 10(b) has its maximum around $|x| \sim 0.4$, whereas $\bar{\Lambda}$ production occurs dominantly in the central region, $|x| \leq 0.4$. The solid lines in Fig. 10(b) show the functional forms $(1-|x|)^1$ for Λ and $(1-|x|)^9$ for $\bar{\Lambda}$ production as given by the CIM.[13] The predicted curves agree qualitatively well with the data of Λ for $|x| > 0.4$ and the data of $\bar{\Lambda}$. On the other hand, the prediction of the quark cascade model[14] explains the data for the small $|x|$ region rather well, but fails in the large-$|x|$ region. We emphasize that in spite of several successful theoretical frameworks,[10-15] it still seems to be necessary to get a deeper understanding of the quark-recombination process for baryon production.

The $p_T{}^2$ distributions for Λ and $\bar{\Lambda}$ are shown in Fig. 10(c); they are very similar and their slopes are equal within errors. The fitted slope values are 2.73 ± 0.21 (GeV/c)$^{-2}$ ($\chi^2/\mathrm{DF} = 9.76/7$) for Λ and 2.66 ± 0.74 (GeV/c)$^{-2}$ (1.02/2) for $\bar{\Lambda}$ at $p_T{}^2 < 1.5$ (GeV/c)^2. For Λ production, a break near 0.6 (GeV/c)^2 is observed. A two-slope-form yields 3.72 ± 0.49 (GeV/c)$^{-2}$ for $p_T{}^2 \leq 0.6$ (GeV/c)^2 and 1.16 ± 0.70 (GeV/c)$^{-2}$ for $0.6 < p_T{}^2 \leq 1.5$ (GeV/c)^2 with $\chi^2/\mathrm{DF} = 2.98/5$. It is interesting to note that a similar slope value, 4.2 ± 0.3 (GeV/c)$^{-2}$, is observed in the $p_T{}^2$ distribution in the reaction $ep \to e + \Lambda + X$, for the events with $p_T{}^2 < 0.8$ (GeV/c)^2.[19]

The momentum-transfer distribution $t' = |t - t_{\min}|$ between the Λ and initial proton is plotted in Fig. 11(a). A sharp break is evident at $t' \approx 1.6$ (GeV/c)^2. The differential distribution was fitted with an exponential form $Ae^{-Bt'}$. The fit yields $A = 4.35 \pm 0.57$ mb/(GeV/c)^2 and $B = 1.33 \pm 0.20$ (GeV/c)$^{-2}$ for $t' \leq 1.5$ (GeV/c)^2, and $A = 0.71 \pm 0.25$ mb/(GeV/c)^2 and $B = 0.31 \pm 0.10$ (GeV/c)$^{-2}$ for $1.5 < t' < 6.0$ (GeV/c)^2. The break at $t' \approx 1.6$ has been reported previously in 12.4- and 200-GeV/c pp interactions.[9] The structure of the t' distribution

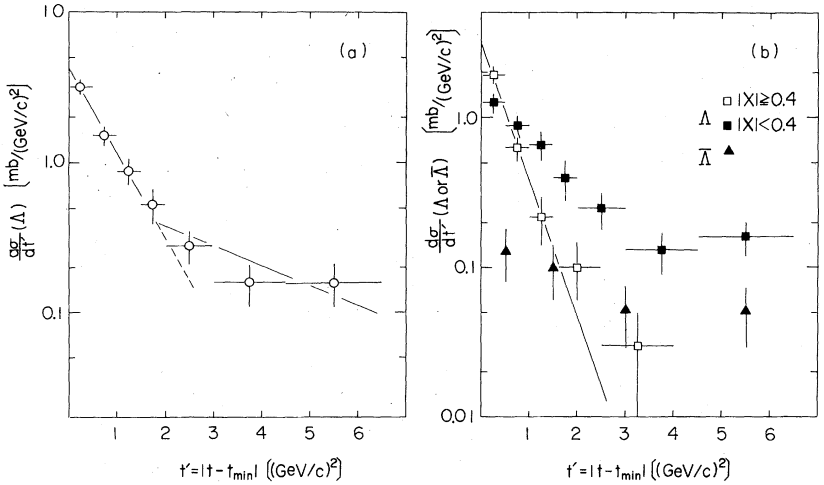

FIG. 11. (a) $d\sigma/dt'$ for inclusive Λ production. (b) $d\sigma/dt'$ for Λ and $\bar{\Lambda}$ as a function of $|x|$. The solid lines in (a) show fits to the data.

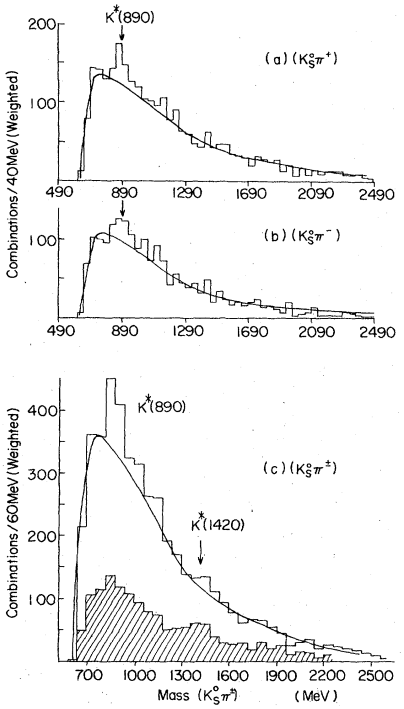

FIG. 12. (a) ($K^0_S\pi^+$) effective-mass distribution and (b) ($K^0_S\pi^-$) effective-mass distribution, both in 40-MeV bin size. (c) The combined mass distribution for ($K^0_S\pi^\pm$) in 60-MeV bin size, where the shaded histogram is for ($K^0_S\pi^\pm$) events having $0.1 < |x| < 0.2$. The background curves are calculated by associating K^0_S's with pions from different events having the same multiplicities as explained in the text.

may indicate two contributions for Λ production, one from fragmentation ($|x| > 0.4$) and the other from central production, as shown in Fig. 11(b). The t' distribution of $\bar{\Lambda}$ shows a more gradual slope due most likely to a central production, corresponding to that for Λ in the region $|x| < 0.4$.

IV. INCLUSIVE $K^*(890)$ AND $K^*(1420)$ PRODUCTION

A. Effective-mass distributions of the ($K^0_S\pi^\pm$) systems

The effective-mass distributions for ($K^0_S\pi^+$) and ($K^0_S\pi^-$) combinations are plotted in Figs. 12(a) and 12(b), where secondary tracks were assigned as pions unless the ionization losses on the tracks were consistent with a proton hypothesis, and only events with $x(K^0_S) < 0.0$ and $x(\pi^\pm) < 0.05$ were used. Clear peaks of $K^{*\pm}(890)$ are observed.

The background is calculated by associating K^0_S's with pions from different events having the same multiplicities. The associated multiplicity distribution for the background events is adjusted to be the same as that of the real events, by weighting each event of multiplicity n_{ch} by a factor of $1/(N-1)$, where N is the number of events of multiplicity n_{ch}. The x and $p_T{}^2$ distributions for the background ($K^0_S\pi^\pm$) systems are also adjusted to be the same as those of the real events. The normalization of the background is made to events in the region of effective mass of the ($K^0_S\pi^-$) mass distribution less than 810 MeV and above 2.0 GeV, where correlations in the ($K^0_S\pi^\pm$) system are expected to be small. This normalization is then applied to the ($K^0_S\pi^\pm$) mass region, 810–970 MeV. The average mass resolution was estimated as

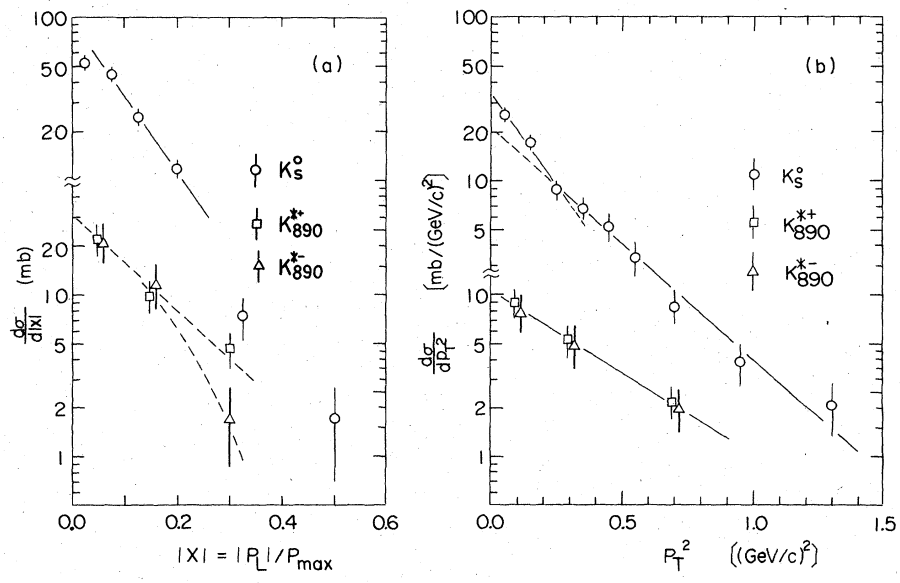

FIG. 13. Differential cross sections for K^0_S and $K^{*\pm}(890)$ production. (a) $d\sigma/d|x|$ and (b) $d\sigma/dp_T{}^2$. The curves in (a) are drawn to guide the eye. The straight lines in (b) show the fits explained in the text.

± 12 MeV for this mass region. After subtraction of the background and correction for the branching ratio $K^{*\pm} \to K^{\pm}\pi^0$, and for the measuring efficiency of secondary tracks (93%), the cross sections of $K^{*+}(890)$ and $K^{*-}(890)$ are obtained to be 4.1 ± 1.0 mb and 3.6 ± 1.0 mb respectively, where systematic errors from the ambiguity of the normalization of the background and statistical errors have been included, the combined errors amounting to 25% in average.

In Fig. 12(c) we plot the combined mass distribution of the $(K^0_S\pi^{\pm})$ systems in 60-MeV bins, to search for evidence for higher mass resonances. A broad bump near 1420 MeV is observed. The peak is more clearly seen if we plot $(K^0_S\pi^{\pm})$ events having $0.1 < |x| < 0.2$, as shown in the shaded histogram. The number of excess events above the background in the mass region, 1300–1540 MeV, is found to be 50 ± 25 weighted combinations, which corresponds to a combined cross section for $K^{*\pm}(1420)$ of 3.4 ± 1.7 mb. Statistical and systematic errors are included, as mentioned above.

B. Inclusive $K^{*\pm}(890)$ spectra

The $|x|$ distributions of $K^{*\pm}(890)$ are shown in Fig. 13(a). Central production of K^{*-} is obvious in comparison with K^{*+} production. In the central region $|x| \leq 0.2$, K^{*+} and K^{*-} mesons are equally produced, and the production ratio K^{*+}/K^{*-} is found to be 0.96 ± 0.30. In the region $0.2 < |x| < 0.4$, this ratio increases to 2.7 ± 1.2. This variation of the charge ratio K^{*+}/K^{*-} as a function of $|x|$ is very similar to the variation of the ratio K^+/K^- observed in 100–400 GeV/c pp interactions,[16] and in ep interactions.[20] This feature of central $K^{*-}(890)$ production is consistent with the quark model,[12] since no common valence quark exists in the initial state for the case of $K^{*-}(890)$ production. The excess of K^{*+} production in the region of $|x| > 0.2$, amounting to 0.6 ± 0.3 mb, is considered to be due to proton fragmentations.

In Fig. 13(b) we also present the $p_T{}^2$ distributions of $K^{*\pm}(890)$ compared with K^0_S data. The $p_T{}^2$ distribution for K^0_S shows a steep exponential slope in the region $p_T{}^2 < 0.3$ (GeV/c)^2 as discussed in Sec. III B. This structure of the $p_T{}^2$ distribution for K^0_S can be attributed to the effect of resonance decay.[1,8] The slope values are obtained as 2.3 ± 0.5 (GeV/c)$^{-2}$ for $K^{*+}(890)$ and 2.2 ± 0.6 (GeV/c)$^{-2}$ for $K^{*-}(890)$ in the region $p_T{}^2 \leq 1.5$ (GeV/c)^2.

C. Production ratios of K^0_S, $K^*(890)$, and ρ^0

In order to see a scaling behavior of K^0_S and $K^{*\pm}(890)$ production, the cross sections for K^0_S and $K^{*\pm}(890)$ as a function of the incident momentum are shown in Fig. 14(a), together with data on ρ^0 production.[4,5] The cross section for K^{*-} increases rapidly with the incident momentum, and becomes comparable with that of K^{*+} production above 100 GeV/c. This feature indicates that the central production becomes dominant in the $K^{*\pm}(890)$ production in the 400-GeV/c

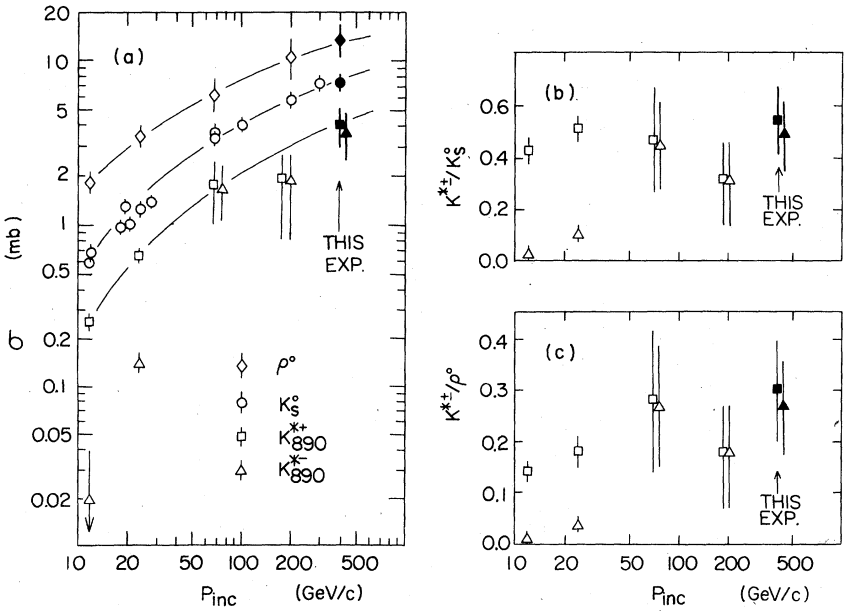

FIG. 14. (a) Inclusive cross sections for K^0_S, $K^{*\pm}(890)$, and ρ^0 production in pp interactions, (b) production ratios $K^{*+}(890)/K^0_S$ and $K^{*-}(890)/K^0_S$, and (c) production ratios $K^{*\pm}(890)/\rho^0$, as a function of incident momentum. The curves in (a) are drawn to guide the eye.

region.

It is interesting to notice that the production ratio K^{*+}/K^0_S seems to have a constant value of 0.40–0.55 over the wide range of momentum from 12 to 405 GeV/c [Fig. 14(b)], whereas the production cross section of K^0_S increases drastically from 0.7 to 7.5 mb. The ratio observed in this experiment is 0.55 ± 0.11. The constancy of the K^{*+}/K^0_S ratio indicates an approximate constancy of the vector/pseudoscalar ratio for strange-meson production in pp interactions. A similar constancy of the ρ^0/π^- ratio, having a value of 0.10–0.13, is observed over a similar momentum range.[1,3,4]

In the additive quark model[10] the production ratios of various particles are predicted under the assumption of statistical equilibrium in high-energy collisions. The probability of strange-quark production is assumed to be suppressed relative to nonstrange-quark production. The empirical suppression factor $\lambda \sim 0.3$ is taken from experimental data on the K/π ratio. The suppression factor λ for strange-quark production in 405-GeV/c pp interactions is estimated to be 0.30 ± 0.10 from the ratio K^{*+}/ρ^0 using our data on ρ^0 production, which are reported elsewhere.[5] The factor λ seems to increase with incident momentum[2] and to reach a constant value of about 0.3 above 100 GeV/c as shown in Fig. 14(c).

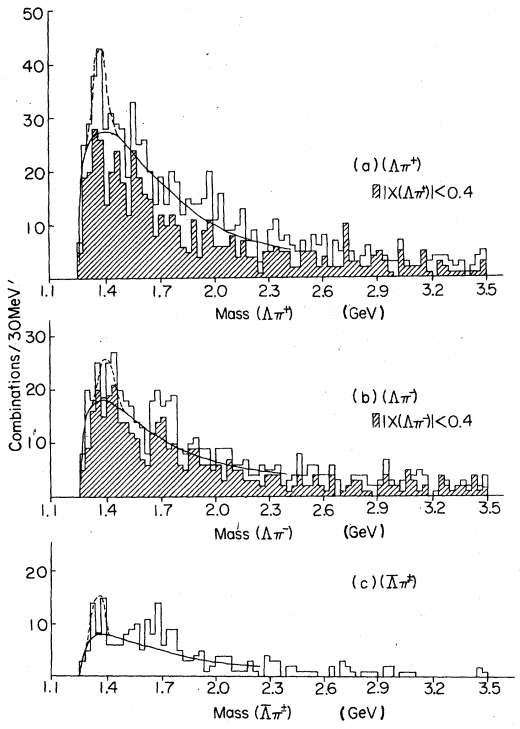

FIG. 15. (a) $(\Lambda\pi^+)$ effective-mass distribution and (b) $(\Lambda\pi^-)$ effective-mass distribution. (c) $(\bar{\Lambda}\pi^\pm)$ effective-mass distribution. The background curves are calculated similarly to those illustrated in Fig. 12.

The experimental production ratios for pseudoscalar, vector, and tensor mesons are found to be 1: 0.52 ± 0.14: 0.23 ± 0.12, assuming $\sigma(M^+) = \sigma(M^-) = \sigma(M^0) = \sigma(\overline{M}^0)$, where M stands for K, $K^*(890)$, and $K^{**}(1420)$. The value of the K^*/K ratio is somewhat smaller than the value 0.7, which is predicted by the additive quark model using $\lambda = 0.3$.[10] In the multiperipheral resonance production model by Fukugita *et al.*,[11] the production ratios for pseudoscalar, vector, and tensor mesons are predicted, based on unitarity and duality, with a consistency relation between two-body scattering and multiparticle production reactions. The predicted values for K, $K^*(890)$, and $K^{**}(1420)$ mesons are 1: 0.53 – 0.62: 0.13 – 0.15, which agree within error with our data.

In summary, the suppression factor λ depends on energy, and reaches a constant value ~0.3 in the 400-GeV/c region. The production ratios for K, K^*, and K^{**} obtained in this and other experiments seem to be energy independent.[1] The multiperipheral resonance production model[11] describes well the production ratios for pseudoscalar, vector, and tensor mesons.

D. Direct production cross sections

Having observed $K^*(890)$ and $K^*(1420)$, we can now discuss the cross sections of directly produced $K^{\pm,0}$, $K^{*\pm,0}(890)$, and $K^{*\pm,0}(1420)$. Disregarding the contribution from the decay of such higher mass resonances as $\phi(1020)$, $f(1514)$, $L(1770)$, etc., and assuming $\sigma(M^+) = \sigma(M^-)$, etc., mentioned above, one may deduce the following relations between observed (σ_{ob}) and direct (σ_d) production cross sections:

$$\sigma^P_{ob} = \sigma^T_d + \sigma^V_d + \sigma^P_d, \quad \sigma^V_{ob} = 0.27 \times \sigma^T_d + \sigma^V_d, \quad \sigma^T_{ob} = \sigma^T_d,$$

where the superscripts P, V, and T correspond to pseudoscalar ($K^{\pm,0}$), vector [$K^{*\pm,0}(890)$], and tensor [$K^{*\pm,0}(1420)$] mesons, respectively. Inserting the corresponding values of observed cross sections, $\sigma^P_{ob} = 7.43 \pm 0.45$ mb, $\sigma^V_{ob} = 3.85 \pm 1.15$ mb, and $\sigma^T_{ob} = 1.7 \pm 0.8$ mb, one can obtain the value for direct production of each multiplet:

$$\sigma^P_d = 2.3 \pm 1.2 \text{ mb}, \quad \sigma^V_d = 3.4 \pm 1.0 \text{ mb}, \quad \sigma^T_d = 1.7 \pm 0.8 \text{ mb}.$$

Since we have neglected any contribution from the decays of higher mass resonances, the true value of σ^P_d would be somewhat smaller than the value obtained here.

This result means that direct pseudoscalar-K-meson production may account for less than one-third of total inclusive kaon production. Evidence of vector-meson dominance in inclusive meson

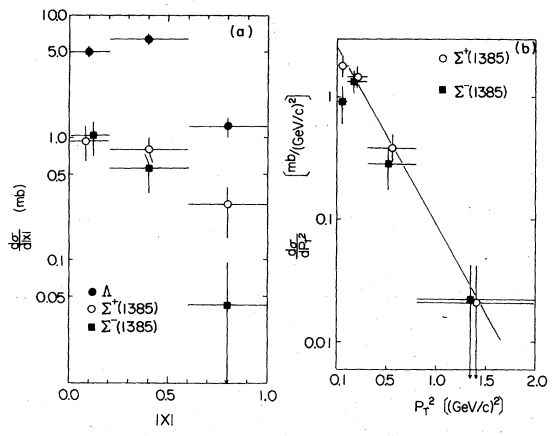

FIG. 16. Differential cross sections for Λ and $\Sigma^{\pm}(1385)$ production. (a) $d\sigma/d|x|$ and (b) $d\sigma/dp_T^2$. The solid line in (b) shows a fit to the data.

production at high energy is suggested. It may also be worth mentioning that a suppression is observed in tensor $K^*(1420)$ meson production, compared with the expected ratios due to the statistical factor $2J+1$, the number of different spin states, in scalar, vector, and tensor mesons. Similar suppression is also observed in data on f/ρ^0 production in pp and πp interactions.[1,5,8] This suppression may be partially due to the effect of the centrifugal barrier in the quark-antiquark recombination processes. This phenomenon has been discussed in the multiperipheral model[11] and in the thermodynamic quark model.[15]

V. INCLUSIVE $\Sigma^{\pm}(1385)$ AND $\overline{\Sigma}^{\pm}(1385)$ PRODUCTION

A. $(\Lambda\pi^{\pm})$ and $(\overline{\Lambda}\pi^{\pm})$ effective-mass distributions

Figures 15(a)–15(c) show the effective-mass distributions of the $(\Lambda\pi^+)$, $(\Lambda\pi^-)$, and $(\overline{\Lambda}\pi^{\pm})$ systems, respectively. The background curves were evaluated by the same method described in Sec. IV A. A sharp peak of $\Sigma^+(1385)$ and somewhat broader bump of $\Sigma^-(1385)$ are observed. An $\overline{\Sigma}^{\pm}(1385)$ peak is also observed in Fig. 15(c). After subtraction of the smoothed background, the corresponding cross sections were determined. The cross sections are $\sigma(\Sigma^+(1385)) = 0.67 \pm 0.12$ mb, $\sigma(\Sigma^-(1385)) = 0.45 \pm 0.09$ mb, and $\sigma(\overline{\Sigma}^{\pm}(1385)) = 0.25 \pm 0.08$ mb, after correction for decay branching ratios. The shaded histograms in Figs. 15(a) and 15(b) indicate the events with $|x| < 0.4$. The cross sections in this $|x|$ region are found to be 0.36 ± 0.08 mb for $\Sigma^+(1385)$ and 0.39 ± 0.09 mb for $\Sigma^-(1385)$.

B. Inclusive $\Sigma^{\pm}(1385)$ spectra

The differential cross sections $d\sigma/d|x|$ and $d\sigma/dp_T^2$ for $\Sigma^{\pm}(1385)$ are shown in Figs. 16(a) and 16(b). $\Sigma^+(1385)$ and $\Sigma^-(1385)$ are equally produced in the central region $|x| < 0.4$, while Σ^- production is considerably suppressed in the region of $|x| > 0.6$. The ratio $\Sigma^+(1385)/\Sigma^-(1385)$ is found to be ~6 for this region. Such a high value is considered as due to the suppression of double charge exchange in the proton fragmentation regions. The excess of the $\Sigma^+(1385)$ cross section over that of $\Sigma^-(1385)$ is about 0.2 mb, corresponding to ~0.1 mb for proton fragmentation.[7]

The p_T^2 distributions for $\Sigma^+(1385)$ and $\Sigma^-(1385)$ are shown in Fig. 16(b). The slope values are found to be 3.34 ± 0.46 $(\mathrm{GeV}/c)^{-2}$ for $\Sigma^+(1385)$ and 3.13 ± 0.52 $(\mathrm{GeV}/c)^{-2}$ for $\Sigma^-(1385)$.

C. Production ratios of strange baryons

In Table IV we show a compilation of the relevant data on $\Sigma^{\pm}(1385)$ production in pp and πp interactions.[7,21-23] This compilation indicates a constancy of the $\Sigma^+(1385)/\Lambda$ production ratio at a value of ~0.17, above 12 GeV/c, and a monotonic increase of the $\Sigma^-(1385)/\Lambda$ ratio. The latter may be understood as due to the increase of the contribution of the central production of $\Sigma^-(1385)$.

In the central region $|x| \leq 0.2$, the $\Sigma^+(1385)/\Lambda$

TABLE IV. Cross sections for $\Sigma^{\pm}(1385)$ production in pp and $\pi^{\pm}p$ interactions.

p_{inc} (GeV/c)	Beam	Λ (mb)	$\Sigma^+(1385)$ (mb)	$\Sigma^-(1385)$ (mb)	$\Sigma^+(1385)/\Lambda$ ratio	$\Sigma^-(1385)/\Lambda$ ratio	Reference
405	p	4.01 ± 0.35	0.67 ± 0.12	0.45 ± 0.09	0.17 ± 0.03	0.11 ± 0.02	This exp.
24	p	1.76 ± 0.06 [e]	0.28 ± 0.03	0.12 ± 0.02	0.16 ± 0.02	0.07 ± 0.01	a
15	π^+	0.95 ± 0.02	0.19 ± 0.04	0.03 ± 0.01	0.20 ± 0.04	0.033 ± 0.012	b
15	π^-	1.27 ± 0.05	0.20 ± 0.03	···	0.16 ± 0.02	···	c
12	p	1.12 ± 0.03 [e]	0.20 ± 0.02	0.07 ± 0.01	0.18 ± 0.02	0.06 ± 0.01	a
6	π^-	0.89 ± 0.11	0.07 ± 0.02	0.09 ± 0.03	0.08 ± 0.02	0.10 ± 0.03	d

[a] K. Böckmann *et al.* (Ref. 7).
[b] C. Baltay *et al.* (Ref. 21).
[c] F. Barriero *et al.* (Ref. 21).
[d] R. Sugahara *et al.* (Ref. 22).
[e] V. Blobel *et al.* (Ref. 23).

and $\Sigma^-(1385)/\Lambda$ ratios are found to be equal to each other at a value of ~0.20, which is consistent with the prediction of the additive quark model.[10] The $\overline{\Sigma}^{\pm}/\overline{\Lambda}$ ratio is found to give the similar value of 0.20 ± 0.07.

VI. SUMMARY AND CONCLUSIONS

We have studied the inclusive production of K^0_S, Λ, $\overline{\Lambda}$, and also of resonances in the reactions $pp \to (K^0_S, \Lambda, \text{ or } \overline{\Lambda}) + \pi^{\pm} + \text{anything}$ at 405 GeV/c. Our main results on resonance production may be summarized as follows:

(i) Inclusive production of strange resonances such as $K^*(890)$, $K^*(1420)$, $\Sigma(1385)$, and $\overline{\Sigma}(1385)$ were observed. The cross sections are determined as 4.1 ± 1.0 mb for $K^{*+}(890)$, 3.6 ± 1.0 mb for $K^{*-}(890)$, 3.4 ± 1.7 mb for $K^{*\pm}(1420)$, 0.67 ± 0.12 mb for $\Sigma^+(1385)$, 0.45 ± 0.09 mb for $\Sigma^-(1385)$, and 0.25 ± 0.08 mb for $\overline{\Sigma}^{\pm}(1385)$.

(ii) The overall production ratios of $K^{*+}(890)/K^0_S$ and $\Sigma^+(1385)/\Lambda$ are obtained to be 0.55 ± 0.14 and 0.17 ± 0.03, respectively. Comparison with the data at lower energies indicates that these ratios are energy independent over the wide range of momentum from 12 to 405 GeV/c.

(iii) The direct production cross sections for pseudoscalar, vector, and tensor K mesons are estimated to be 2.3 ± 1.2 mb, 3.4 ± 1.0 mb, and 1.7 ± 0.8 mb, respectively. Direct pseudoscalar-K-meson production accounts for less than one-third of total inclusive kaon production. Evidence of vector-meson dominance in inclusive meson production at high energy is indicated. A suppression is observed in tensor $K^*(1420)$ meson production, compared with the expected ratios due to the statistical factor $2J+1$, the number of different spin states.

In the study of single-particle spectra of K^0_S, Λ, and $\overline{\Lambda}$ production, the following conclusions were obtained:

(iv) The average numbers of K^0_S, Λ, and $\overline{\Lambda}$ increase linearly as a function of $\ln(s)$, where s is the c.m. energy squared. The ratios of the slope parameters are found to be 1: 0.18 ± 0.10: 0.13 ± 0.04. The rapidity distributions give similar values for the production ratios of K^0_S, Λ, and $\overline{\Lambda}$ in the central region $|y_{\text{c.m.}}| \leq 1.2$, 1: 0.19 ± 0.04: 0.13 ± 0.03 at 405 GeV/c. These ratios are consistent with the values predicted by the additive quark model, 1: 1/6: 1/6, for meson/baryon/antibaryon in the central region. The suppression factor λ for strange-quark production is estimated to be 0.30 ± 0.10 at 405 GeV/c from the observed ratio $K^{*+}(890)/\rho^0$. The factor λ seems to increase with incident momentum and to reach a constant value of 0.3 above 100 GeV/c.

(v) The $|x|$ distributions for K^0_S and Λ production are described qualitatively well with the power behaviors $E^* d\sigma/d|x| \propto (1 - |x|)^{2p-3}$ predicted by the constituent-interchange model, although discrepancies are observed in the central region, $|x| < 0.1$ for K^0_S and $|x| < 0.4$ for Λ.

ACKNOWLEDGMENTS

We are very grateful to Professor J.C. Vander Velde of University of Michigan and Professor T. Ferbel of Rochester University for letting us use the 405- GeV/c pp film taken at the Fermilab 30-in. hydrogen bubble chamber. We are also grateful to the Fermi National Accelerator Laboratory for granting us the present analysis of this film. Both groups at KEK and OCU are much obliged to their scanning and measuring staff for their patient works. One of the authors (K.T. at KEK) would like to thank Professor J. Arafune for various discussions.

[1] W. Kittel, in *Proceedings of the VIII International Symposium on Multiparticle Dynamics, Kaysersberg, 1977*, edited by P. Schübelin (CRN, Strasbourg, 1977); A. Ziminski, in *Proceedings of the 1977 European Conference on Particle Physics, Budapest*, edited by L. Jenik and I. Montvag (CRIP, Budapest, 1978); P. Schmid, in *Proceedings of the XVIII International Conference on High Energy Physics, Tbilisi, 1976*, edited by N. N. Bogulobov *et al.* (JINR, Dubna, U.S.S.R., 1977) Vol. I, p. A2–9.

[2] K. Böckmann, University of Bonn Report No. Bonn-HE-77-24, invited report at the International Symposium on Hadron Structure and Multiparticle Production, Kazimierz, Poland, 1977 (unpublished).

[3] J. Whitmore, Phys. Rep. 10C, 273 (1974); 27C, 187 (1976).

[4] V. Blobel *et al.*, Phys. Lett. 48B, 73 (1974); V. V. Ammosov *et al.*, Yad. Fiz. 24, 59 (1976) [Sov. J. Nucl. Phys. 24, 30 (1976)]; R. Singer *et al.*, Nucl. Phys. B135, 265 (1978); G. Jancso *et al.*, *ibid.* B124, 1 (1977); R. Singer *et al.*, Phys. Lett. 60B, 385 (1976).

[5] H. Kichimi *et al.*, Lett. Nuovo Cimento 24, 129 (1979); A. Suzuki *et al.*, *ibid.* 24, 449 (1979).

[6] F. T. Dao *et al.*, Phys. Rev. Lett. 30, 34 (1973); J. P. DeBrion *et al.*, *ibid.* 34, 910 (1975); S. J. Barish *et al.*, Phys. Rev. D 12, 1260 (1975); F. T. Dao *et al.*, in *Proceedings of the XIX International Conference on High Energy Physics, Tokyo, 1978*, edited by S. Homma, M. Kawaguchi, and H. Miyazawa (Phys. Soc. of Japan, Tokyo, 1979).

[7] H. Kichimi *et al.*, Phys. Lett. 72B, 411 (1978); K. Böckmann *et al.*, Nucl. Phys. B143, 395 (1978).

[8] M. Deutchman *et al.*, Nucl. Phys. B103, 426 (1976); J. Bartke *et al.*, *ibid.* B107, 93 (1976); F. C. Winkel-

mann *et al.*, Phys. Lett. 56B, 101 (1975); C. Evangelista *et al.*, *ibid.* 70B, 373 (1977).
[9]J. W. Chapman *et al.*, Phys. Lett. 47B, 465 (1973); Margaret Alston-Garnjost *et al.*, Phys. Rev. Lett. 35, 142 (1975); K. Jaeger *et al.*, Phys. Rev. D 11, 1756 (1975); K. Jaeger *et al.*, *ibid.* 11, 2405 (1975); A. Sheng *et al.*, *ibid.* 11, 1733 (1975).
[10]V. V. Anisovich and V. M. Shekhter, Nucl. Phys. B55, 455 (1973).
[11]M. Fukugita *et al.*, Nucl. Phys. B121, 93 (1977); Phys. Rev. D 19, 187 (1979).
[12]R. D. Field and R. P. Feynman, Phys. Rev. D 15, 2590 (1977); Wolfgang Ochs, Nucl. Phys. B118, 397 (1977).
[13]S. J. Brodsky and J. F. Gunion, Phys. Rev. D 17, 848 (1978); K. P. Das and R. C. Hwa, Phys. Lett. 68B, 459 (1977); R. Blankenbecler and S. J. Brodsky, Phys. Rev. D 10, 2973 (1974); S. J. Brodsky and G. R. Farrar, Phys. Rev. Lett. 31, 1153 (1973).
[14]H. Fukuda and C. Iso, Prog. Theor. Phys. 57, 483 (1977).
[15]H. Bohr and H. B. Nielsen, Nucl. Phys. B128, 275 (1977).
[16]J. R. Johnson *et al.*, Phys. Rev. Lett. 39, 1173 (1977); Phys. Rev. D 17, 1292 (1978).
[17]C. Bromberg *et al.*, Phys. Rev. Lett. 31, 1563 (1973).
[18]R. T. Edwards *et al.*, Phys. Rev. D 18, 76 (1978).
[19]I. Cohen *et al.*, Phys. Rev. Lett. 40, 1614 (1978).
[20]J. F. Martin *et al.*, Phys. Rev. Lett. 40, 283 (1978).
[21]F. Barriero *et al.*, Phys. Rev. D 17, 669 (1978); C. Baltay *et al.*, Columbia University report (unpublished).
[22]R. Sugahara *et al.*, Nucl. Phys. (to be published).
[23]V. Blobel *et al.*, Nucl. Phys. B69, 454 (1974).